



FDM FABRICATED PLA PARTS: AN EXPERIMENTAL STUDY OF EFFECT OF PROCESS PARAMETERS ON MECHANICAL PROPERTIES UNDER COMPRESSIVE AND FLEXURAL LOADING

Shailendra Kumar, Soham Teraiya, Vishal Kumar Koriya

Department of Mechanical Engineering, Sardar Vallabhbhai National Institute of Technology,
Surat, Gujarat, India-395007

Corresponding author: Shailendra Kumar, skbudhwar@med.svnit.ac.in

Abstract: The present paper describes an experimental investigation on mechanical properties of poly-lactic-acid (PLA) parts under compressive and flexural loading. The PLA parts are fabricated by fused deposition modelling (FDM) technique. In present work, effect of raster angle, raster width and infill density on strength and modulus of parts under compressive and flexural loading is studied. It is found that infill density affects compressive strength and modulus of parts significantly under compressive loading. Compressive properties increase with increase in infill density. Further, it is found that raster width and infill density significantly influence flexural strength and modulus. Flexural properties increase with increase in infill density, and decrease in decrease in raster width. Further, predictive models are developed for responses, and process parameters are optimized using genetic algorithm to maximize the responses.

Keywords: process parameters, mechanical properties, PLA, FDM, strength, modulus

1. INTRODUCTION

Fused deposition modeling (FDM) is most widely used rapid prototyping (RP) technique due to its ability to produce high strength polymer parts (Bakar et al, 2010; Pacurar et al., 2010; Cotoros et al., 2012; Butt et al., 2020). FDM parts are extensively employed in sports, electronics, aerospace, architecture, automobile, robotic and pharmaceutical sectors, etc. (Jin et al., 2015; Kuo et al., 2017). In FDM, heated material is deposited on a print bed in layer-wise fashion. Various materials namely, polyamide (PA), polylactic acid (PLA), polypropylene (PP), acrylonitrile-butadiene-styrene (ABS) and polycarbonates (PC), are used for printing of the parts (Cousins, 2002; Aziz et al., 2020). PLA is most widely used material because it is biodegradable and easier to print. Mechanical performance of FDM fabricated parts is affected by several process parameters such as, part orientation, slice height, raster angle, number of contours, contour width, nozzle

temperature, raster width, nozzle diameter, bed temperature, printing speed, infill density, etc. (Chaturvedi, 2009; Peng et al, 2010; Harris et al., 2019; Shanmugam et al., 2021; Ali et al., 2022; Teraiya et al., 2022). Therefore, it is important to investigate their effects on mechanical properties of FDM parts.

Several studies have been reported for investigating mechanical performance of FDM fabricated parts under static and dynamic loading conditions. Hambali et al. (2010) investigated influence of build direction on ABS brackets fabricated by material extrusion technique. They found that an optimized build orientation is significantly improves mechanical properties of ABS parts. Tian et al. (2016) studied flexural properties of composite PLA parts and observed that, with increase in slice height and raster angle, flexural strength decreases. Mohamed et al. (2016) found that air gap, slice height, build orientation and shell numbers significantly affects dynamic flexural modulus of part. Mishra et al. (2017) reported that number of shells, build direction, and air gap affects compressive strength of FDM parts significantly. Chacon et al. (2017) suggested that FDM part possess maximum mechanical properties, when it is printed at on-edge build direction. Garg et al. (2017) suggested that mechanical strength is maximized at optimum raster angle of 0°. Balderrama-Armendariz et al. (2018) found that build direction and raster angle significantly influence shear properties of parts. Rajpurohit and Dave (2018a) investigated influence of raster width, raster angle, and slice height on tensile strength of PLA specimens and, reported that mechanical performance of specimens is significantly influenced by all parameters except slice height. Also, they reported that slice thickness and raster width negatively correlated with flexural strength (Rajpurohit et al., 2018b). Chadha et al. (2019) found

that flexural properties of part can be tailored by varying infill pattern. Vyavahare and Kumar (2020) reported that compressive strength of re-entrant structures decreases with decrease slice height. Dev et al. (2021) optimized process parameter of FDM for flexural strength using RSM-GA. Kumar et al. (2021) found that infill density and slice height significantly affects compressive properties, while there was no significance of raster angle. Pawar et al. (2021) reported that flexural strength decreases with decrease in infill density while, surface finish increases decrease in slice height. Bardiya et al. (2021) investigated the effect of slice height, build direction and infill percentage on flexural properties and reported significant improvement in strength at higher values of selected process parameters. Saad et al. (2021) investigated the influence of print speed, layer height, print temperature and contour speed on flexural strength of PLA parts using response surface methodology. They further optimized the process parameters using particle swarm optimization method to maximize the flexural strength. Tanveer et al. (2022) reported that parts have higher strength when printed in horizontal orientation along with 100 % infill. Dixit et al. (2022) studied compressive behavior of PLA and TPU material, and found slice height and infill density affects compressive strength of part significantly. Mohan et al. (2022) studied relationship between build direction and infill density, and flexural, tensile, hardness, impact and wear strength of PLA specimens and, found that maximum mechanical strength of parts of achieved with 100% infill density. El Magri et al. (2022) investigated influence of extrusion temperature, material deposition speed, and slice height on tensile strength. They reported that modulus proportionately vary with extrusion temperature. Majority of researchers have studied the tensile properties of thermoplastic polymer parts fabricated by FDM. However, few efforts have been applied for investigating effects of process parameters namely, raster angle, raster width and infill density on compressive and flexural properties of parts. Therefore, in the present study, experimental work is performed to fulfill this research gap. Predictive models are developed for all responses. Further, process parameters are optimized by genetic algorithm (GA) using MATLAB to maximize the responses.

2. MATERIALS AND METHODS

Methodology of present work includes selection of material, design of experiments, computer aided

design (CAD) modeling, fabrication of specimens, and measurement of responses.

2.1. Material

PLA is a thermoplastic monomer emanating from organic sources such as, corn starch and sugar cane. Being a non-toxic and biodegradable material, it is best suited for making food grade utensils and medical devices including screws, pins, plates and rods. For present investigation, a PLA is used as feedstock material. Material properties of PLA are given in Table 1 (Lanzotti et al., 2015)

Table 1. Material properties of PLA

Properties	Values
Chemical formula	(C ₃ H ₄ O ₂) _n
Density	1.24 g/cm ³
Glass transition temperature	50-80 °C
Printing temperature	190-220 °C
Heat deflection temperature	49-52 °C at 0.46 MPa
Flexural yield strength	65-85 MPa
Tensile strength	60-66 MPa

2.2. CAD Modelling

Computer aided design (CAD) models of specimens for compression and flexural testing are developed using Autodesk Inventor 2022 as shown in Figure 1. Size of the specimen for compressive and flexural loading are decided on the basis of ASTM D695 and ASTM D790 respectively.

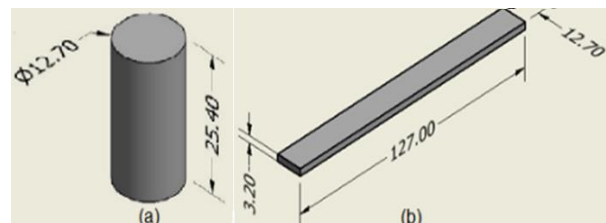


Fig. 1. CAD model of specimen - (a) compressive loading, and, (b) flexural loading

2.3. Experimental plan

In present study, influence of three process parameters namely raster angle, raster width and infill density, on compressive strength, compressive modulus, flexural strength and flexural modulus is investigated. Range of process parameters are given in Table 2. Constant parameters for printing of parts are listed in Table 3. With the help of Design Expert software, central composite design (CCD) is employed to prepare experimental plan. As experimental design is face centered CCD, α value is taken as 1. Experimental design includes 6 center points, 8 factorial points and 6 axial or star points.

Finally, design suggests a total of 20 experimental runs.

Parameters	Levels		
	-1	0	+1
Raster angle(°)	30	45	60
Raster width(mm)	0.25	0.35	0.45
Infill density(%)	40	70	100

Parameters	Levels
Print temperature (°C)	220
Build orientation	Horizontal
Print speed (mm/sec)	40
Slice height (mm)	0.25
Infill pattern	Cross grid
Bed temperature (°C)	70
Number of contours	2

2.4. Fabrication of Specimen

According to experimental plan, all PLA parts are fabricated using FDM machine (M/s Wasp, Italy, Model: 2040 Turbo 2). The STL file of CAD model is fed into the Ultimaker Cura software which generates G-codes by slicing the 3D model into 2D layers. Each layer is a combination of rasters which is deposited on print bed using heated extruder. Feed stock material with diameter of $\varnothing 1.75\text{mm}$ is fed to the machine in a filament form. Total 40 parts are fabricated for compression and flexural testing, as shown in Figure 2.



(a)



(b)

Fig. 2. FDM fabricated parts for (a) compression testing (b) flexural testing

2.5. Measurement of Responses

2.5.1. Compression testing

Electronic tensometer (Model PC 2000) is used for compressive testing of specimen. Machine have load capacity of 20 kN with load accuracy of 1% and least count 0.05% of load cell. As tensometer can only pull the specimen, a fixture is used for compression testing as shown in Figure 3. The parts are compressed at a rate of 1.3 mm/min. Load vs displacement data is extracted from machine in the form of excel sheet. Compressive strength (σ_{CY}) and compressive modulus (E_C) is determined using Eq. 1 and Eq. 2 respectively.

$$\sigma_{C,Y} = \frac{P_Y}{\pi r^2} \quad (1)$$

$$E_C = \frac{\sigma_1 - \sigma_2}{\varepsilon_1 - \varepsilon_2} \quad (2)$$

where: $\sigma_{C,Y}$ = compressive strength (MPa); E_C = compressive modulus (MPa); P_Y = peak load at yielding (N); r = radius of specimen (6.35 mm); σ_1 = maximum stress within proportional limit; σ_2 = minimum stress within proportional limit; ε_1 , ε_2 = corresponding strains at σ_1 and σ_2 .

2.5.2. Three-point flexural testing

Computerized Micro UTM (Model KIC-2-100-C) is used for three-point flexural testing of specimen as shown in Figure 4. Loading capacity of machine is 10 kN with accuracy of 0.5% and least count of 1% of load cell. For testing of specimen under flexural loading, a customized fixture is designed and fabricated using FDM as shown in Figure 5. For 3-point flexural testing, each specimen is first marked by a line at half of its length and at a span length of 51 mm (25.5 mm each side of center point) so that it is easy to locate the specimen between the fixtures. Load-displacement values are exported into excel sheet and values of flexural stress (σ_f) and flexural modulus has been calculated using Eq. 3 and Eq. 4.

$$\sigma_f = \frac{3PL}{2bd^2} \quad (3)$$

$$E_f = \frac{\sigma_1 - \sigma_2}{\varepsilon_1 - \varepsilon_2} \quad (4)$$

where: P = peak load (MPa); L = support span length (51 mm); d = depth or thickness of specimen (3.2 mm); b = width of specimen (12.7 mm); σ_f = flexural stress in the outer fibers at mid-point (MPa); E_f = flexural modulus (MPa); σ_1 = maximum stress within proportional limit; σ_2 = minimum stress within proportional limit; ε_1 , ε_2 = corresponding strains at σ_1 and σ_2 .



Fig. 3. Compression testing of specimen using fixture

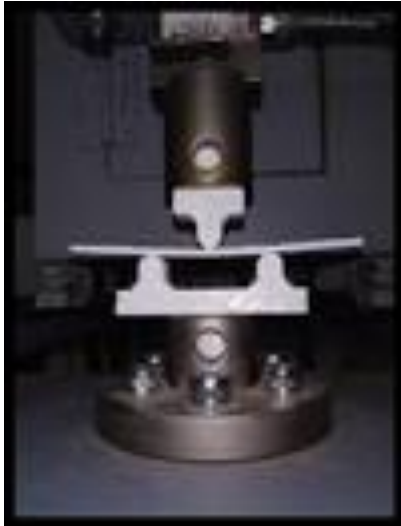


Fig. 4. FDM fabricated PLA part under flexural testing

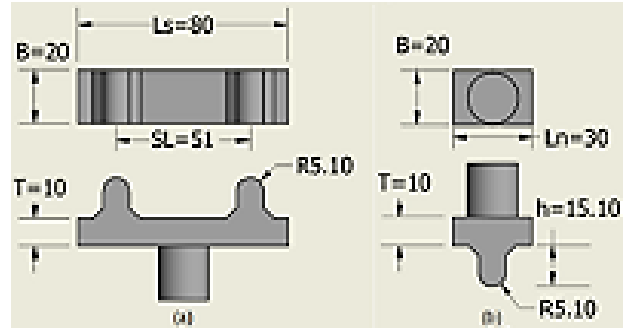


Fig. 5. Three-point flexural testing fixture, (a) support fixture and (b) loading nose fixture

3. RESULTS AND DISCUSSION

Table 4 lists experimental results for compressive and flexural loading of FDM fabricated parts.

3.1 Mechanical properties of FDM fabricated parts under compressive loading

Typical stress vs strain curve for compression tested specimen of Run 2 are shown in Figure 6. It is observed that specimen is elastically deformed till strain of 0.08 (Point C). With further increase in compression load, specimen starts to deform plastically (Point D). After strain of 0.3, stresses exponentially increase with further increase in strain, which results in densification of compression tested part.

Table 4. Experimental results

Run	A (°)	B mm	C %	$\sigma_{c,y}$ MPa	E_c MPa	σ_f MPa	E_f MPa
1	45	0.25	70	42.19	660.512	60.59	2112.23
2	45	0.35	70	38.01	577.413	54.71	2202.45
3	45	0.35	70	37.78	638.563	59.41	2373.71
4	60	0.45	40	22.14	495.932	38.82	1770.86
5	30	0.45	100	97.16	1035.73	65.88	2451.96
6	30	0.35	70	39.41	662.854	52.94	2285.65
7	60	0.45	100	91.43	891.594	76.47	2451.96
8	60	0.35	70	31.74	539.319	58.24	2369.12
9	45	0.35	40	20.13	358.318	40.00	2132.52
10	60	0.25	40	21.91	379.342	40.59	1906.66
11	45	0.35	70	34.61	616.094	58.24	2270.46
12	45	0.45	70	41.11	623.9	47.65	1889.53
13	60	0.25	100	89.96	880.625	84.71	3055.73
14	30	0.25	100	83.54	959.497	77.65	3115.65
15	30	0.45	40	20.36	373.535	32.35	1337.43
16	45	0.35	70	41.96	683.765	52.35	2087.09
17	45	0.35	70	41.42	654.216	55.29	2357.65
18	45	0.35	70	37.16	621.787	52.94	2210.72
19	45	0.35	100	97.63	1053.22	74.12	3086.54
20	30	0.25	40	20.13	361.213	38.82	1786.13

A: Raster angle, B: Raster width, C: Infill density

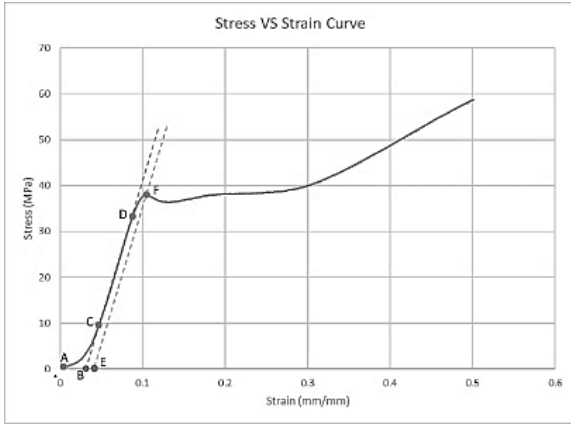


Fig. 6. Stress-strain curve of Run 2

Experimental results are analyzed using analysis of variance (ANOVA). As per Table 5, infill density influences compressive strength and modulus of FDM fabricated parts significantly. Figure 7 depicts impact of process parameters on strength and modulus of compression tested specimens. It is found that, strength and modulus decrease with decrease in infill density. With increase in infill density, distance between adjacent raster decreases, resulting in decrease in size of voids and airgaps. Due to decrease in size of voids, strength of inter-layer and inter-raster bonding is improved. Therefore, compressive properties of part improve at high infill density. Similar trend has been observed by Kumar et al. (2020) for compressive strength of ABS parts. Compressive properties increase with increase in raster angle till 45° , thereafter it starts to decrease.

Rasters printed with angle less than 45° are aligned nearer to axis of loading resulting in buckling of rasters. However, rasters printed with angle greater than 45° tends to tear due to lateral displacement of material under compressive loading.

Table 5. ANOVA for Compressive Strength and modulus

	Compressive strength		Compressive modulus	
	F	p	F	p
A-Raster Angle	0.0906	0.7696	1.55	0.2418
B-Raster Width	1.64	0.2297	1.18	0.3038
C-Infill Density	984.11	< 0.0001	296.72	< 0.0001
AB	1.44	0.2575	0.0693	0.7976
AC	0.0801	0.7830	6.03	0.0340
BC	2.09	0.1789	0.0793	0.7840
A ²	3.63	0.0858	1.27	0.2860
B ²	0.8278	0.3843	0.0307	0.8644
C ²	79.06	< 0.0001	4.79	0.0535

Further, it is found that, strength and modulus slightly decrease with decrease in raster width. It is because, thicker raster has larger cross-sectional area, which increases ability of a part to take higher compressive loads. However, with increase in raster width, size of inter-raster and inter-layer void increases, resulting in decrease in strength. Therefore, these two phenomena nullify each other's effect, resulting in slight change in compressive properties of part. Similar trend was observed by Romeijn et al., (2020) while studying mechanical properties of FDM parts.

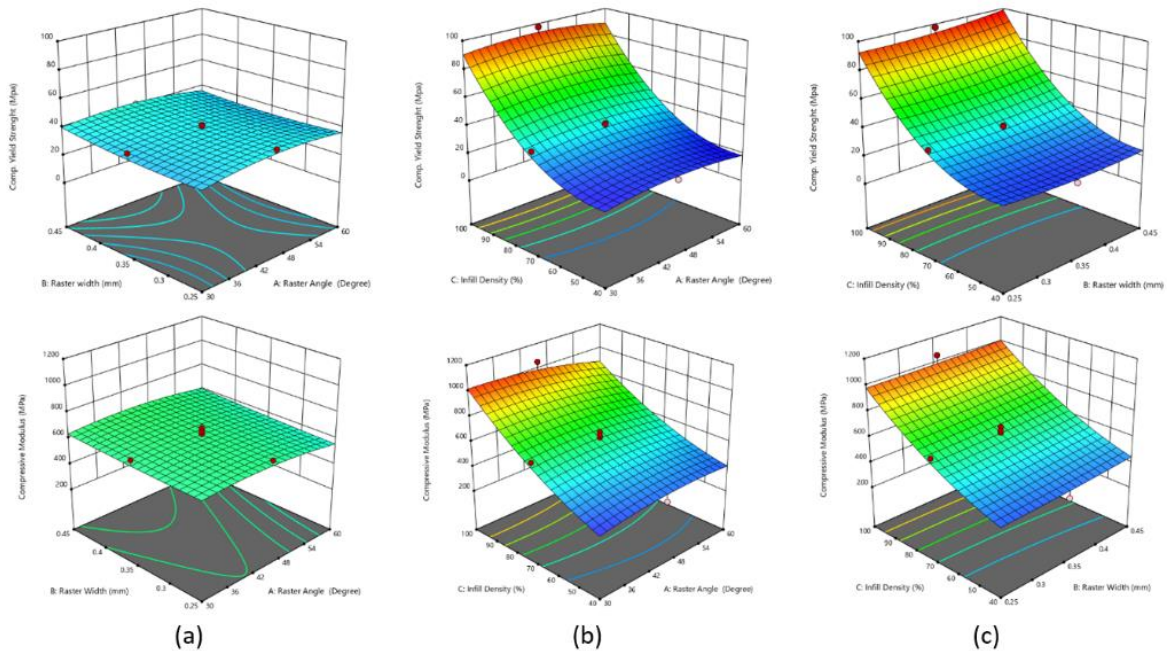


Fig. 7. Influence of - (a) Raster angle and Raster width, (b) Raster angle and Infill density, and (c) Raster width and Infill density, on strength and modulus under compressive loading

3.2 Mechanical properties of FDM fabricated parts under flexural loading

Stress-strain curve for flexural loading of specimen of Run 17 is shown in Figure 8. Initially, till strain of 0.02, specimen deforms elastically. On further application of flexural load, plastic deformation of specimen is initiated. At strain of 0.045, fracture is observed at outer most layer of specimen, resulting in decrease in stresses. Point *Y* and point *B* denotes the maximum strength and strength at break, respectively.

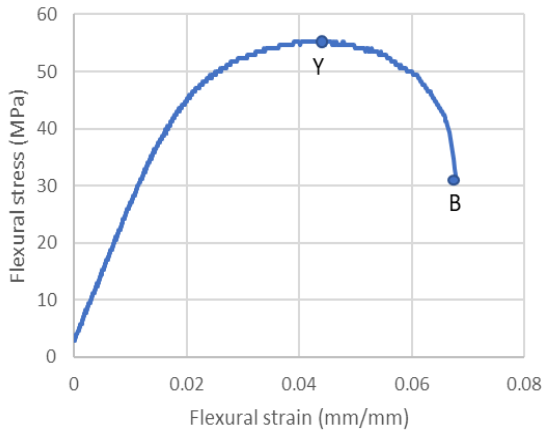


Fig. 8. Stress vs Strain curve for Run 17

Table 6 lists ANOVA for strength and modulus of flexural tested parts. It is found that strength is significantly affected by all process parameters while

flexural modulus is influenced by raster width and infill density. Effect of process parameters on flexural properties are depicted in Figure 9. With increase in raster angle, flexural strength increases. Length of the rasters increase with increase in raster angle. During flexural loading, long rasters can bear high loads as compared to short rasters. Further, it is noticed that flexural strength and modulus decrease with increase in raster width. With decrease in raster width, number of rasters required to print a layer increase. Therefore, strength and modulus increase due to increase in number of inter-raster bond. Further, with decrease in raster width, size of inter-raster voids decreases, resulting in further improvement in flexural properties of specimen.

Table 6. ANOVA for flexural strength and modulus

	Strength		Modulus	
	F	p	F	p
A-Raster Angle	15.47	0.0028	2.96	0.1159
B-Raster Width	26.99	0.0004	38.25	0.0001
C-Infill Density	564.07	< 0.0001	242.89	< 0.0001
AB	1.35	0.2723	1.54	0.2424
AC	1.76	0.2138	4.19	0.0680
BC	2.75	0.1280	5.18	0.0461
A ²	0.1130	0.7437	0.0028	0.9588
B ²	0.4056	0.5385	25.51	0.0005
C ²	1.71	0.2198	19.92	0.0012

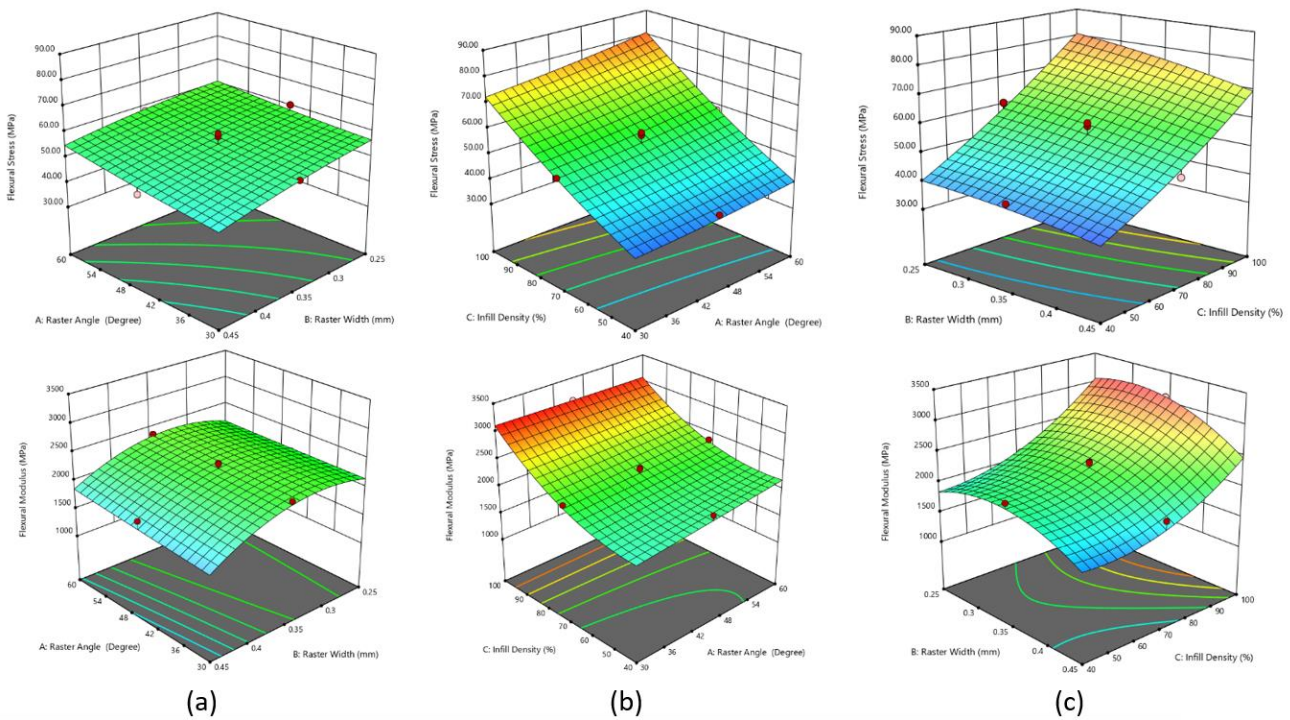


Fig. 9. Influence of - (a) Raster angle and Raster width, (b) Raster angle and Infill density, and (c) Raster width and Infill density, on strength and modulus under flexural loading

Moreover, it is found that, as infill density decreases, flexural strength and modulus decrease. With increase in infill density, distance between adjacent raster decreases, resulting in decrease in size of voids and airgaps. Bonding strength of raters increase due to decrease in inter-raster distance, resulting in improved flexural properties of specimen at high infill density. Chicos et al., (2022) observed identical

trend for mechanical properties of polyamide composite parts.

Also, predictive models are developed for all responses as given in Table 7. As R^2 values for each model is above 0.90, it can be concluded that regression models accurately predict the strength and modulus of specimen.

Table 7. Regression models for responses

Response	Regression model	R^2
Compressive Strength	$\sigma_{c,y} = 40.0653 + 2.03309 \times A - 120.079 \times B - 1.97918 \times C - 1.01293 \times A \times B - 0.000795725 \times A \times C + 0.609701 \times B \times C - 0.0182841 \times A^2 + 196.371 \times B^2 + 0.0213222 \times C^2$	0.9911
Compressive Modulus	$E_C = -218.555 + 18.7931 \times A - 232.313 \times B + 3.91253 \times C + 3.25007 \times AB - 0.100983 \times AC - 1.73782 \times BC - 0.15817 \times A^2 + 553.159 \times B^2 + 0.0767691 \times C^2$	0.9689
Flexural Strength	$\sigma_f = 27.0514 - 0.418574 * A + 29.635 * B + 0.373595 * C + 0.686285 * AB + 0.00261442 * AC - 0.490204 * BC + 0.00225791 * A^2 - 96.2582 * B^2 + 0.00219849 * C^2$	0.9840
Flexural Modulus	$E_f = -1505.52 + 3.55927 * A + 21137.8 * B - 9.35412 * C + 31.0673 * AB - 0.170522 * AC - 28.4569 * BC + 0.0150433 * A^2 - 32312.1 * B^2 + 0.31725 * C^2$	0.9704

3.3. Optimization of parameters using GA

Using genetic algorithm, optimization of process parameters is performed to maximize compressive strength, compressive modulus, flexural strength and flexural modulus. In present multi-objective multi-variable optimization, quad-objective triple-variable problem (Eq. 5 to Eq. 8) is solved using genetic algorithm solver. Minus sign is assigned to all objective functions to convert them from minimization to the maximization problem.

$$\text{Maximize } F_1 = -\sigma_{c,y} (A, B, C) \quad (5)$$

$$\text{Maximize } F_2 = -E_C (A, B, C) \quad (6)$$

$$\text{Maximize } F_3 = -\sigma_f (A, B, C) \quad (7)$$

$$\text{Maximize } F_4 = -E_f(A, B, C) \quad (8)$$

subject to

$$30 \leq A \leq 60$$

$$0.25 \leq B \leq 0.45$$

$$40 \leq C \leq 100$$

Among 1000 iterations, a solution with desirability of 0.9175 is selected. It is observed that optimum values of raster angle, raster width and infill density are 53.9° , 0.31 mm and 99.94% respectively, while maximum values of $\sigma_{c,y}$, E_C , σ_f and E_f are 91.0 MPa, 930.3 MPa, 80.7 MPa and 3130.6 MPa respectively. The set of solutions obtained from the iterations are shown in pareto charts in Figure 10. A trail of points at the bottom of graph shows the convergence of solution. It is observed that overall desirability is

0.9175 (Figure 11), which is near to 1, therefore acceptable.

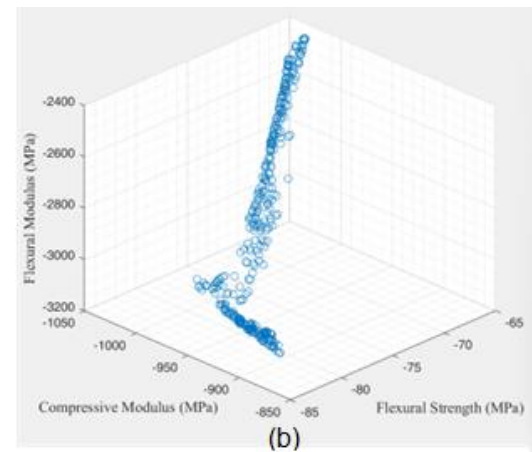
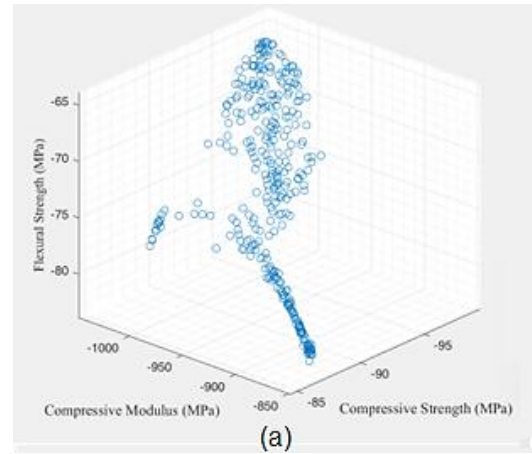


Fig. 10. Pareto chart showing set of solutions for optimization problem

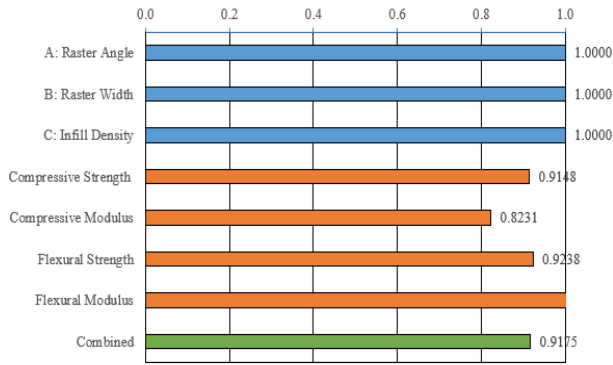


Fig. 11. Desirability bar graph.

3.4. Confirmation test

Confirmation tests have been performed for randomized and optimized value of parameters to validate regression model and optimization results. Results of confirmation tests along with their predicted values and percentage difference are given in Table 8. Deviation is less than 10 % than predicted and optimized values, therefore it can be concluded that confirmation test results are in good agreement with regression model and optimization results.

Table 8. Results of confirmation tests

Levels	A (°)	B (mm)	C (%)	$\sigma_{C,Y}$ (MPa)			E_C (MPa)			σ_f (MPa)			E_f (MPa)		
				Pred.	Obs.	% Diff.	Pred.	Obs.	% Diff.	Pred.	Obs.	% Diff.	Pred.	Obs.	% Diff.
Optimized	53.8	0.31	99.94	91.03	95.52	4.932	930.26	953.71	2.520	80.72	82.97	2.787	3130.6	3019.8	3.53
Random	40	0.3	60	28.70	30.12	4.925	536.66	501.95	6.468	50.16	46.38	7.536	2126.3	1954.7	8.06
	50	0.4	80	53.59	52.87	1.338	731.03	803.76	9.948	60.67	63.77	5.110	2305.9	2189.6	5.043

A= Raster angle, B= Raster width, C= Infill density, Pred= Predicted values, Obs= Observed values, % Diff= percentage difference

4. CONCLUSION

In the present study, an investigation has been performed to study effects raster angle, raster width and infill density on compressive and flexural properties of FDM fabricated PLA parts. It is observed that infill density affects compressive modulus and strength of FDM fabricated parts significantly. Also, compressive properties decrease with decrease in infill density. Also, compressive properties increase with increase in raster angle till 45°, thereafter it starts to decrease. Further, it is found that compressive strength and modulus slightly increases with increase in raster width. Flexural strength is influenced by all process parameters while flexural modulus is influenced by raster width and infill density. With increase in raster angle and infill density flexural strength increases. Further, it is found that flexural strength and modulus decrease with increase in raster width.

Further, predictive models are developed for responses. Also, process parameters are optimized using genetic algorithm to maximize the responses. Findings of this study are useful in determining the value of process parameters to maximize compressive and flexural properties of FDM fabricated PLA parts.

5. REFERENCES

1. Ali, H. B., Oleiwi, J. K., & Othman, F. M. (2022). *Compressive and Tensile Properties of ABS Material as a Function of 3D Printing Process*

Parameters, *Revue des Composites et des Matériaux Avancés*, 32(3).

2. Aziz, R., Haq, M. I. U., & Raina, A. (2020). *Effect of surface texturing on friction behaviour of 3D printed polylactic acid (PLA)*, *Polymer Testing*, 85, 106434.
3. Bakar, N. S. A., Alkahari, M. R., & Boejang, H. (2010). *Analysis on fused deposition modelling performance*, *Journal of Zhejiang University-Science A*, 11(12), 972-977.
4. Balderrama-Armendariz, C. O., Macdonald, E., Espalin, D., Cortes-Saenz, D., Wicker, R. & Maldonado-Macias, A. (2018). *Torsion Analysis of the Anisotropic Behavior of Fdm Technology*, *The international journal of advanced manufacturing technology*, 96, 307-317.
5. Bardiya, S., Jerald, J., & Satheeshkumar, V. (2021). *The impact of process parameters on the tensile strength, flexural strength and the manufacturing time of fused filament fabricated (FFF) parts*, *Materials Today: Proceedings*, 39, 1362-1366.
6. Butt, J., & Bhaskar, R. (2020). *Investigating the effects of annealing on the mechanical properties of FFF-printed thermoplastics*, *Journal of Manufacturing and Materials Processing*, 4(2), 38.
7. Chacón, J. M., Caminero, M. A., García-Plaza, E., & Núñez, P. J. (2017). *Additive manufacturing of PLA structures using fused deposition modelling: Effect of process parameters on mechanical properties and their optimal selection*, *Materials & Design*, 124, 143-157.

8. Chadha, A., Haq, M. I. U., Raina, A., Singh, R. R., Penumarti, N. B., & Bishnoi, M. S. (2019). *Effect of fused deposition modelling process parameters on mechanical properties of 3D printed parts*, World Journal of Engineering, 16(4), 550-559.
9. Chaturvedi, V. (2009). *Parametric optimization of fused deposition modeling using response surface methodology*, Doctoral Thesis, available at http://ethesis.nitrkl.ac.in/1497/1/M.Tech._thesis_vedansh.pdf
10. Chicos, L.A., Pop, M.A., Zaharia, S.M., Lancea, C., Buican, G.R., Pascariu, I.S. and Stamate, V.M. (2022). *Infill Density Influence on Mechanical and Thermal Properties of Short Carbon Fiber-Reinforced Polyamide Composites Manufactured by FFF Process*, Materials, 15(10), 3706.
11. Cotoros, D., Baritz, M., (2012). *Implementing rapid prototyping technologies for corrective insoles*, International Journal of Modern Manufacturing Technologies, 4, 41-46.
12. Cousins, K. (2002). *Polymers in building and construction*, iSmithers Rapra Publishing, 13(10), Shropshire, United Kingdom.
13. Dev, S., & Srivastava, R. (2021). *Optimization of fused deposition modeling (FDM) process parameters for flexural strength*, Materials Today: Proceedings, 44, 3012-3016.
14. Dixit, N., & Jain, P. K. (2022). *Effect of Fused Filament Fabrication Process Parameters on Compressive Strength of Thermoplastic Polyurethane and Polylactic Acid Lattice Structures*, Journal of Materials Engineering and Performance, 1-10.
15. El Magri, A., Ouassil, S. E., & Vaudreuil, S. (2022). *Effects of printing parameters on the tensile behavior of 3D- printed acrylonitrile styrene acrylate (ASA) material in Z direction*, Polymer Engineering & Science, 62(3), 848-860.
16. Garg, A., Bhattacharya, A. & Batish, A. (2017). *Failure Investigation of Fused Deposition Modelling Parts Fabricated at Different Raster Angles under Tensile and Flexural Loading*, Proceedings of the Institution of Mechanical Engineers, Part B: Journal of Engineering Manufacture, 231, 2031-2039.
17. Hambali, R.H., Celik, H., Smith, P., Rennie, A., & Ucar, M. (2010). *Effect of Build Orientation on Fdm Parts: A Case Study for Validation of Deformation Behaviour by FEA*, Proceedings of international conference on design and concurrent engineering, Universiti Teknikal Malaysia Melaka, Melaka, 224-228.
18. Harris, M., Potgieter, J., Archer, R., & Arif, K. M. (2019). *Effect of material and process specific factors on the strength of printed parts in fused filament fabrication: A review of recent developments*, Materials, 12(10), 1664.
19. Jin, Y. A., He, Y., Xue, G. H., & Fu, J. Z. (2015). *A parallel-based path generation method for fused deposition modeling*, The International Journal of Advanced Manufacturing Technology, 77(5), 927-937.
20. Kumar, M. A., Khan, M. S., & Mishra, S. B. (2020). *Effect of machine parameters on strength and hardness of FDM printed carbon fiber reinforced PETG thermoplastics*, Materials Today: Proceedings, 27, 975-983.
21. Kumar, N., & Kumar Jain, P. (2021). *Analysing the influence of raster angle, slice height and infill rate on the compressive behaviour of EVA through CNC-assisted fused layer modelling process*, Proceedings of the Institution of Mechanical Engineers, Part C: Journal of Mechanical Engineering Science, 235(10), 1731-1740.
22. Kuo, C. C., Chen, C. M., & Chang, S. X. (2017). *Polishing mechanism for ABS parts fabricated by additive manufacturing*, The International Journal of Advanced Manufacturing Technology, 91(5), 1473-1479.
23. Lanzotti, A., Grasso, M., Staiano, G., & Martorelli, M. (2015). *The impact of process parameters on mechanical properties of parts fabricated in PLA with an open-source 3-D printer*, Rapid Prototyping Journal, 21(5), 604-617.
24. Mishra, S. B., Abhishek, K., Satapathy, M. P., & Mahapatra, S. S. (2017). *Parametric appraisal of compressive strength of fdm build parts*, Materials Today: Proceedings, 4(9), 9456-9460.
25. Mohamed, O. A., Masood, S. H., & Bhowmik, J. L. (2016). *Mathematical modeling and FDM process parameters optimization using response surface methodology based on Q-optimal design*, Applied Mathematical Modelling, 40(23-24), 10052-10073.
26. Mohan, E., & Saravana Kumar, M. (2022). *Experimental investigation on mechanical and tribological properties of the fused filament fabrication of poly-lactic acid parts with various print orientations*, Applied Physics A, 128(5), 1-14.
27. Pacurar, R., Balc, N., & Olimpia, R. (2010). *Improving the accuracy of the SLS metal parts using the Finite Element Method*, International Journal of Modern Manufacturing Technologies, 2(1), 61-66.
28. Pawar, S., & Dolas, D. (2021). *Effect of process parameters on flexural strength and surface roughness in fused deposition modeling of PC-ABS material*, Journal of Micromanufacturing, 25165984211031115.
29. Peng, A. H., & Wang, Z. M. (2010). *Researches into influence of process parameters on*

- FDM parts precision*, Applied Mechanics and Materials. Trans Tech Publications Ltd, 34, 338-343
30. Rajpurohit, S. R., & Dave, H. K. (2018a). *Effect of process parameters on tensile strength of FDM printed PLA part*, Rapid Prototyping Journal, 24(8), 1317-1324.
31. Rajpurohit, S. R., & Dave, H. K. (2018b). *Flexural strength of fused filament fabricated (FFF) PLA parts on an open-source 3D printer*, Advances in Manufacturing, 6(4), 430-441.
32. Romeijn, T., Wells, B., Wei, D., & Paul, G. (2020). *Investigation into the shear property of thin-walled additively manufactured structures using staggered fused filament fabrication*, Additive Manufacturing, 35, 101259.
33. Saad, M. S., Mohd Nor, A., Zakaria, M. Z., Baharudin, M. E. & Yusoff, W. S. (2021). *Modelling and Evolutionary Computation Optimization on Fdm Process for Flexural Strength Using Integrated Approach Rsm and Pso*, Progress in Additive Manufacturing, 6, 143-154.
34. Shanmugam, V., Rajendran, D. J. J., Babu, K., Rajendran, S., Veerasimman, A., Marimuthu, U., & Ramakrishna, S. (2021). *The mechanical testing and performance analysis of polymer-fibre composites prepared through the additive manufacturing*, Polymer testing, 93, 106925.
35. Tanveer, M. Q., Mishra, G., Mishra, S., & Sharma, R. (2022). *Effect of infill pattern and infill density on mechanical behaviour of FDM 3D printed Parts-a current review*, Materials Today: Proceedings, 62(1), 100-108.
36. Teraiya, S., Vyavahare, S., & Kumar, S. *Parametric investigation for mechanical properties of tetra- anti- chiral auxetic structures of polymer under compressive loading*, Polymer Engineering & Science, 62(6), 1735-1755.
37. Tian, X., Liu, T., Yang, C., Wang, Q., & Li, D. (2016). *Interface and performance of 3D printed continuous carbon fiber reinforced PLA composites*. Composites Part A: Applied Science and Manufacturing, 88, 198-205.
38. Vyavahare, S., & Kumar, S. (2020). *Re-entrant auxetic structures fabricated by fused deposition modeling: An experimental study of influence of process parameters under compressive loading*, Polymer Engineering & Science, 60(12), 3183-3196.

Received: June 15, 2022 / Accepted: December 15, 2022 / Paper available online: December 20, 2022 © International Journal of Modern Manufacturing Technologies